Energy forecasting and optimization for wastewater treatment facility: A hybrid machine learning – Metaheuristic scenario based approach

Energy Reports 15 (2026) 108940

Contents lists available at ScienceDirect

Energy Reports

journal homepage: www.elsevier.com/locate/egyr

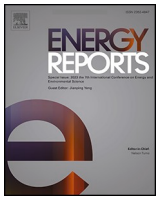

Research paper

Energy forecasting and optimization for wastewater treatment facility: A hybrid machine learning – Metaheuristic scenario based approach

Alireza Ahmadi [a], Mahmood Abdoos [a], Ali Roghani Araghi [a,b,*], Amir Ali Saifoddin [a,**]

[a] School of Energy Engineering and Sustainable Resources, College of Interdisciplinary Science and Technology, University of Tehran, Tehran, Iran
[b] Department of Mechanics and Maritime Sciences, Chalmers University of Technology, Gothenburg, Sweden

ARTICLE INFO

Keywords:
Machine Learning
Metaheuristic
Wastewater treatment
Renewable energy

ABSTRACT

Meeting the energy demands of high-consumption facilities, such as wastewater treatment plants (WWTPs), is essential for sustainable urban growth. This study evaluates renewable energy supply strategies through three deterministic models (HOMER software) and a stochastic hybrid machine learning–metaheuristic framework. The deterministic models produced Levelized Costs of Energy (LCOE) of 0.14 $/kW and 0.284 $/kW, while the stochastic model yielded a significantly higher 8.41 $/kW, underscoring the impact of uncertainty on economic feasibility. The hybrid model revealed that battery integration is negligible unless renewable electricity purchase prices rise to 0.45 $/kW, compared to the grid price of 0.036 $/kW (with a hypothetical sellback price of 0.035 $/kW). These findings demonstrate that while deterministic models provide optimistic baselines, the stochastic approach offers a more risk-aware perspective, highlighting the importance of uncertainty modeling in WWTP energy planning. The study contributes a novel methodological framework that integrates machine learning with metaheuristic optimization, offering transferable insights for optimizing renewable integration in high-demand facilities worldwide.

1. Introduction

The escalating scarcity of freshwater resources, driven by climate change, rapid economic development, population growth, and unsustainable water consumption, poses a severe challenge to global water security. Projections indicate a 1 % annual increase in water demand across all sectors (Viet et al., 2019), intensifying pressure on already stressed water supplies. In alignment with the United Nations SDGs particularly SDG 6 (Clean Water and Sanitation) and SDG 12 (Responsible Consumption and Production) enhancing wastewater treatment and reuse is critical for achieving water sustainability (Dange et al., 2025). With an estimated 300 billion cubic meters of wastewater generated annually (Zhang et al., 2024), harnessing this vast resource through advanced treatment technologies is imperative. These technologies must not only be reliable, energy-efficient, and adaptable to varying influent conditions but also capable of producing high-quality effluent with minimal environmental impact while integrating seamlessly with existing infrastructure (Elnakar and Buchanan, 2019).

In a study, Ahmadi and colleagues stated that guaranteeing stable electricity and heating in remote rural areas poses a significant challenge. Renewable hybrid systems are often recommended for this purpose. However, maintaining sustainability requires a connection to the electricity grid, which necessitates purchasing power from power plants that are significant sources of pollution, or deploying extensive equipment to ensure system sustainability (Ahmadi et al., 2025). The mentioned study examines four climatic regions in Iran and evaluates the choice between two storage systems battery-hydrogen and battery-flywheel through a two-stage simulation and optimization process (Ahmadi et al., 2025). The findings indicate that the battery-hydrogen system is significantly more cost-effective, saving up

Abbreviation: SDGS, Sustainable Development Goals; NPC, Net Present Cost; COE, Cost of Electricity; LCOE, Levelized Cost of Electricity; WWTPs, Wastewater Treatment Plants; PV, Photovoltaic; MBRs, Membrane Bioreactors; NZE, Net Zero Energy; SBR, Sequencing Batch Reactor; AI, Artificial intelligence; ML, Machine Learning; SVR, Support Vector Regression; WT, Wind Turbine; SCOE, System's Cost of Energy; RF, Renewable Fration; CV, Cross-Validation; CRF, Capital Recovery Factor; DC, Direct Current; AC, Alternating Current.

* Corresponding author at: School of Energy Engineering and Sustainable Resources, College of Interdisciplinary Science and Technology, University of Tehran, Tehran, Iran.
** Corresponding author.
E-mail addresses: ali.roghani@ut.ac.ir, ali.roghani@chalmers.se (A. Roghani Araghi), saifoddin@ut.ac.ir (A.A. Saifoddin).

https://doi.org/10.1016/j.egyr.2025.108940
Received 17 August 2025; Received in revised form 9 November 2025; Accepted 21 December 2025
Available online 4 February 2026

Table 1
Summary of the regional works about the economic optimization of the hybrid systems (Rad et al., 2020a).

Analyzed hybrid system	Locations (Peak of the load)	Approaches	Size of the optimum system	Results	Ref
PV/WT/DG/Battery	Damghan (1 kW)	HOMER software	PV: 1430 kWh/yr WT: 8353 kWh/yr DG: 3009 kWh/yr	COE: 0.338 $/kWh RF: 76.5 %	(Razmjoo and Davarpanah, 2019)
PV/WT/ DG/Electrolyzer/HT/ Battery/ Boiler	Bandar Abbas, Shiraz, Tabriz, Tehran, Yazd (370.34 kW)	HOMER software	For Tehran: PV: 997 kW WT: 7 units with 95 kW DG: 1000 kW Electrolyzer: 120 kW HT: 130 kg Battery: 9 units with 130 kWh	For Tehran: COE: 0.340 $/kWh RF: 24.7 %	(Akhtari and Baneshi, 2019)
PV/FC/Electrolyzer/HT/DG	Kerman (55 kW)	Multi-objective crow search algorithm	PV: 443 units with 0.26 kW DG: 30 units with 1.8 kW FC: 7 units with 2 kW Electrolyzer: 26 units with 2 kW HT: 4 units with 6 kg	NPC: 1.201 M$	(Jamshidi and Askarzadeh, 2019)
PV/WT/FC/Electrolyzer/HT/ Battery	Kerman (3.3 kW)	HCHSA algorithm	PV: 7 units with 0.120 kW WT: 6 units with 1 kW Battery: 7 units with 1.35 kWh	Life cycle cost: 4000 $	(Zhang et al., 2018)
PV/WT/Biodiesel generator/ Battery	Fedeshk, South Khorasan (7.5 kW)	Hybrid algorithm	PV: 77 m2 (about 48 units with 0.26 kW) Battery: 29 units with 2.1 kWh Biodiesel Generator: 9.875 kW	Life cycle cost: 20,534 $	(Guangqian et al., 2018)
PV/WT/Battery	Tehran (28.1 kW)	GA-PSO/MOPSO/HOMER software	PV: 82 kW WT: 25 kW Battery: 190 kWh	NPC: 787,193 $ COE: 0.508 $/kWh	(Ghorbani et al., 2018)
PV/WT/Battery	Tehran (3.4 kW)	HOMER software	PV: 4 kW WT: 2 kW Battery: 6 units with 7386 kWh	NPC: 20,527 $ COE: 0.258 $/kWh	(Mohammadi et al., 2018)
PV/DG/FC/Electrolyzer/HT/ Battery	Tehran (8.5 kW)	HOMER software	DG: 5 kW PV: 8 kw Battery: 6 units with 7.21 kWh	NPC: 79,895 € COE: 0.316 €/kWh RF: 42 %	(Mehrpooya et al., 2018)
PV/Battery	Birjand (19 kW)	Artificial bee swarm optimization	PV: 418.2 m2 (about 261 units with 0.26 kW) Battery: 5299 units with 2.1 kWh	Life cycle cost: 451,730 $	(Maleki et al., 2017)
PV/WT/DG/Electrolyzer/HT/ Battery	Tehran (1.5 kW)	HOMER software	WT: 4 units with 2.5 kW DG: 1 kW Electrolyzer: 1 kW Battery: 15 units with 9645 kWh	NPC: 63,190 $ COE: 0.783 $/kWh	(Fazelpour et al., 2016)
PV/Biogas generator	Bardsir (230 kW)	HS-GA-PSO algorithms	PV: 521 m2 (about 319 units with 0.235 kW) Biogas Generator: 184.28 kW	NPC: 1.672 M$ COE: 0.185 $/kWh	(Heydari and Askarzadeh, 2016)
PV/Biogas generator/DG/Grid	Golshan (57.87 kW)	HOMER software	PV: 63 kW DG: 25 kW with two generator units Biogas Generator: 10 kW Net Grid Supply: 39,120 kWh	NPC: 398,151 $ COE: 0.193 $/kWh RF: 50.65 %	(Kasaeian et al., 2019)
PV/FC/Electrolyzer/HT/ Battery	Taleghan (5.2 kW)	HOMER software	PV: 10 kW Electrolyzer: 3.5 kW FC: 0.4 kW HT: 2.4 kg Battery: 60 units with 100 Ah	NPC: 237,509 $ IC: 193,563 $	(Shiroudi et al., 2013)
PV/DG/Battery	Kerman (18 kW)	A optimization algorithm based on LPSP	PV: 154 units with 0.080 kW DG: 14 kW with three generator units	COE: 0.438 $/kWh RF: 50 %	(Baniasad Askari and Ameri, 2011)

(*continued on next page*)

Table 1 (*continued*)

Analyzed hybrid system	Locations (Peak of the load)	Approaches	Size of the optimum system	Results	Ref
PV/DG/WT/Battery	Rayen (79.56 kW)	HOMER software	PV: 28.7 kW WT: 14 units with 1.5 kW DG: 30 kW Battery: 18 units with 7.55 kWh	NPC: 268,592 $ COE: 0.197 $/kWh RF: 67.3 %	(Jahangir et al., 2019)
PV/WT/WEC/Battery	Anzali, Genaveh, Jask (8258.16 kW)	HOMER software	For Anzali: PV: 7221 kW WT: 14 units with 660 kW Battery: 454 units with 167 Ah	NPC: 48.8 M$ COE: 0.242 $/kWh RF: 100 %	(Jahangir et al., 2020)
PV/Battery/Grid	Tehran, Tabriz, Shiraz, Isfahan, Mashhad (1.5 kW)	Teaching-learning-based optimization algorithm	For Shiraz: PV: 2.39 kW Battery: 4 kWh	NPC: 24,065 $ COE: 0.175 $/kWh RF: 43.2 %	(Ashtiani et al., 2020)

to $211,327 in NPC and $0.738 in COE. Furthermore, the battery-hydrogen system demonstrates a greater reliance on renewable energy sources, increasing by up to 23.6 % compared to the battery-flywheel system (Ahmadi et al., 2025).

Present WWTPs are typically energy-intensive, which require high investments and operation costs (Hao et al., 2015). Among the current methods, combining PV technology with wastewater treatment shows great promise to achieve these goals (Alvarez-Guerra et al., 2011). The maturity and reliability of the technology also need to be carefully considered. A comprehensive evaluation of the feasibility of constructing PV-supported WWTPs is crucial and requires in-depth research and a systematic approach. Achieving the optimal operation of wastewater treatment plants requires solving the large-scale nonlinear optimization problem caused by complex biochemical reactions (Du and Peng, 2023).

The peak electricity consumption occurs during biological treatment processes, especially within activated sludge systems. In these systems, the energy used for aerating bioreactors accounts for approximately 50–70 % of the total energy expenditure (Masłoń et al., 2020).

Another study stated that in China, significant differences in climatic conditions, levels of economic development, treatment processes used, and population density inevitably lead to regional patterns in energy recovery and consumption of WWTPs. In the aforementioned study, the geographical distribution of energy self-sufficiency of urban wastewater treatment plants in China was investigated based on the NZE model. The results showed that only 19 % of the surveyed WWTPs could generate enough energy to compensate for their energy consumption under their existing operating conditions. The maximum self-sufficiency rate among all the surveyed WWTPs in eastern China was 186.43 %. Their wastewater treatment operation strategies are not conducive to energy recovery. Thirty percent of the surveyed WWTPs could achieve 100 % energy self-sufficiency by adjusting their metabolic substrate allocation (Xiong et al., 2021). Furthermore, wastewater remains largely underutilized as a source of thermal energy (Nowak et al., 2015). Research conducted by Puchwala and Kotas demonstrated that raw wastewater has the potential to recover heat, meeting 98 % of the thermal energy requirements for a SBR. This finding underscores the viability of utilizing wastewater as a significant source of thermal energy in treatment processes (Pochwała and Kotas, 2018).

Bogdanov et al. have conducted a research by using LUT university energy system transition modeling tool resulted that the power and heat in Kazakhstan can move to be completely based on renewable sources by 2050 with a levelized cost of electricity of 45 $€/MWh$ Bogdanov et al. (2019).

AI has emerged as a transformative force in environmental engineering, offering innovative solutions to complex environmental challenges (Talaie et al., 2024). From air pollution monitoring and water resource management to waste management, climate change mitigation, and ecological preservation, AI is revolutionizing the way we address environmental issues (Talaie et al., 2024). Machine learning, neural networks, and other AI technologies are enabling more accurate predictions, optimizing resource use, and improving conservation efforts (Talaie et al., 2024).

To strengthen the background and situate our contribution within existing research, Table 1, providing a comparative perspective that highlights both methodological approaches and reported outcomes.

This research addresses a critical gap in evaluating the techno-

Fig. 1. Study area of Lusail Qatar treatment plant.

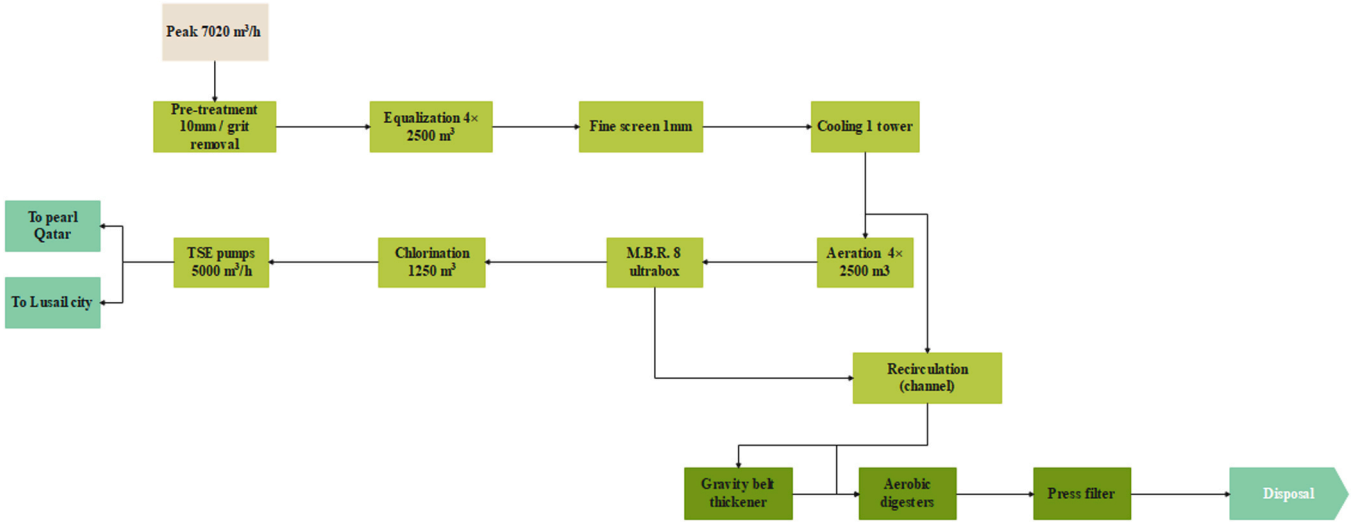

Fig. 2. Flow diagram of the energy requirement of the treatment plant.

economic implications of integrating renewable energy sources into wastewater treatment systems. While most existing studies rely on deterministic, software-based evaluations that assume fixed conditions, such approaches often overlook the uncertainty and variability inherent in real-world operations. Our study systematically compares deterministic modeling (via HOMER software) with stochastic, data-driven methods that couple machine learning algorithms (SVR, Random Forest, Gradient Boosting) with the Jaya metaheuristic optimization algorithm. Using real-world data from Lusail, Qatar, we analyze four scenarios to demonstrate how combining deterministic and stochastic perspectives can provide a more comprehensive understanding of cost-effectiveness and sustainability in high-demand facilities.

2. Methodology

In this section, the methods are completely explained:

2.1. Study area

The following information is gathered from official reports. Fig. 1 shows that the WWTP in Lusail is designed for the reuse of wastewater in the development of residential and commercial buildings in the Lusail area.

The wastewater treatment plant includes the installation of a 12-kilometer collection system to transport sewage from the new city to the treatment station. The recycled water from this facility enables the irrigation of vegetation and the maintenance of green spaces throughout the Pearl artificial island, thereby mitigating desertification effects.

Fig. 2 outlines the process flow for a wastewater treatment plant in Lusail, Qatar. The system handles an average inflow of 60,000 m^3 /day (2500 m^3/hour) with a peak flow rate of 7020 m^3 /hour which corresponds to a population equivalent of 200,000 people. It utilizes aerobic digestion for sludge stabilization and filter presses for dewatering. The needed energy for the desalination plant is about 30,000 kWh/day with a load peak of 2291.5 kW.

The electricity price used in this study (0.036 $/kWh) is based international energy price databases (e.g., GlobalPetrolPrices). This value reflects the average grid electricity cost applicable to high-consumption facilities such as wastewater treatment plants. In contrast, the sellback rate applied in the analysis is a hypothetical assumption introduced for scenario exploration, as Qatar currently does not have a formal feed-in tariff or sellback policy for renewable electricity. This assumption was necessary to evaluate the potential impact of future pricing structures on the economic viability of distributed renewable energy systems.

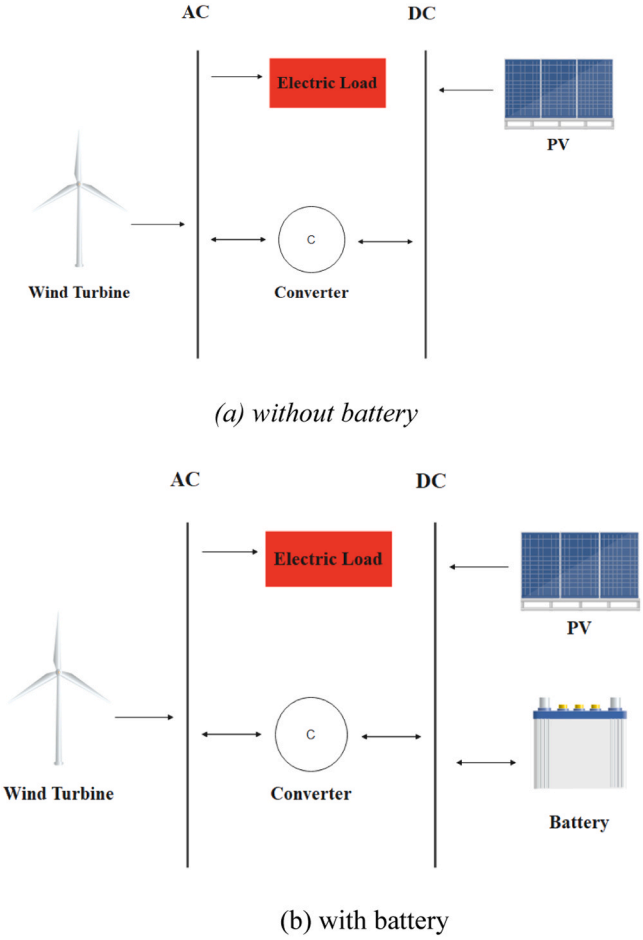

Fig. 3. the hybrid renewable suppliers: (a) without battery (b) with battery.

2.2. The studied software

HOMER Pro is a sophisticated software tool designed for optimizing microgrids and hybrid power systems, particularly those incorporating renewable energy sources such as solar and wind (Qiblawey et al., 2022). This software facilitates the technical and economic analysis of various energy configurations, enabling users to determine the most

Table 2
Details of system components.

System Devices	Power (kW)	Life Time (years)	Efficiency (%)	Capital ($)	Replacement ($)	Maintenance ($/year)
Photovoltaic	0.45	25	24	990	990	10
Wind Turbine	1500	20	40	3000000	3000000	30000
Battery	1	10	95	178	150	12.5
Converter	1	15	95	300	300	10

cost-effective solutions for energy generation and consumption (He et al., 2018). The designed systems are shown in Fig. 3 and Table 2.

2.3. Simulation mathematical expression

A rise in solar cell temperature (T_c) adversely impacts PV efficiency. Therefore, when estimating hourly PV power output (Eq. (1)) it is essential to account for both the PV cell temperature (Eq. (2)) and the corresponding changes in module efficiency (Eq. (3)). In these formulations, P_{PV}denotes the power output of the module, while Y_{PV}refers to its nominal capacity (kW). $G_T$and $G_{T,STC}$represent the actual and standard test condition solar irradiance on the module surface (kW/m^2), respectively. The module derating factor is indicated by f_{PV} (%), and μsignifies the temperature-to-power sensitivity (%/°C). STC stands for standard test conditions. Additionally, $\eta$is the efficiency (%), $T_a$and $V$are the ambient temperature (°C) and wind speed (m/s) under real conditions. NOCT refers to the nominal operating cell temperature, ψ is the correction factor for potential cooling effects, α indicates the solar absorptance of the PV module (%), and $\tau$is the transmittance of the PV cover (%). D_{AC} represents the peak hourly AC bus demand (kW), and σ_{sf} is the inverter safety margin (%) (Rad et al., 2024).

$$P_{PV} = Y_{PV} f_{PV}\left(\frac{G_T}{G_{T,STC}}\right)\left[1+\mu\left(T_C - T_{C,STC}\right)\right] \tag{1}$$

$$\eta_{PV} = \eta_{PV,STC}\left(1+\frac{\mu}{\eta_{PV}}\left(T_a - T_{STC}\right)+\frac{\mu}{\eta_{PV,STC}}\frac{a+bV_{NOCT}}{a+bV}\frac{NOCT-20}{800}\right.$$
$$\left.\left(1-\eta_{PV,STC}\right)G_T\right)\Psi \tag{2}$$

$T_{c,NOCT}$ and $T_{a,NOCT}$ refer to the cell and ambient temperatures, respectively, under nominal operating cell conditions (20 °C). Moreover, $\eta_{mp,STC}$indicates the photovoltaic module's efficiency at its maximum power point (%), αrepresents the solar absorptance of the module (%), and τdenotes the transmittance of any protective cover placed over the PV array (%) (Rad et al., 2020b):

$$T_C = \frac{T_a + \left(T_{C,NOCT} - T_{a,NOCT}\right)\left(\frac{G_T}{G_{T,STC}}\right)\left(\frac{\left[1-\eta_{mP,STC}\left(1-\mu T_{C,STC}\right)\right]}{\alpha\tau}\right)}{1+\left(T_{C,NOCT}-T_{a,NOCT}\right)\left(\frac{G_T}{G_{T,STC}}\right)\left(\frac{\mu\eta_{mP,STC}}{\alpha\tau}\right)} \tag{3}$$

$T_{c,NOCT}$ represents the nominal operating temperature of the panel, typically 45 °C, while $T_{a,NOCT}$ denotes the standard ambient temperature, set at 25 °C. The parameter $\eta_{mp,STC}$ refers to the panel's efficiency at its maximum power output under standard test conditions. Additionally, α is the absorption coefficient of the solar cell surface, and τ indicates the transmittance of the panel's surface coating. The optimal orientation of the photovoltaic panel is determined based on the surface azimuth angle (γ), zenith angle (θ_z), solar azimuth angle (γ_s), and the module tilt angle (β), as outlined in Eq. 4 (Sadeghitabar et al., 2025).

$$COS\theta = Sin\theta_z Sin\beta Cos(\gamma_s - \gamma) + Cos\theta_z Cos\beta \tag{4}$$

Inverters serve the function of transforming DC generated by solar panels into AC, ensuring a stable power supply to end-users, storage systems, and other electrical devices. They also perform the reverse conversion from AC to DC when needed. The inverter capacity is determined using Eq.5: (Sadeghitabar et al., 2025)

$$C_{inv} = \left(\frac{L_{AC}}{\eta_{con}}\right)\sigma_{sf} \tag{5}$$

In this formulation, L_{AC} represents the peak current load passing through the inverter (kW), η_{inv} indicates the inverter's efficiency, typically rated at 95 %, and σ_{sf} stands for the reliability factor (%) used to safeguard against overloading. The inverter's output power is determined based on the manufacturer-specified efficiency and the real-time input power ($P_{inv.in}$), as expressed in Eq. 6 (Sadeghitabar et al., 2025).

$$P_{inv.out} = \eta_{inv} P_{inv.in} \tag{6}$$

Battery charging and discharging behavior can be assessed at each time step using Eqs. 7 and 8. In these equations, SOC indicates the battery's state of charge (%), σrefers to the internal discharge rate of the battery system, D_{load} denotes the energy demand (kWh), $P_{Ren}$is the renewable power generated, and P_{bat} represents the available energy within the battery bank. Additionally, η_{bat} defines the nominal efficiency of the storage system, while C and D correspond to the charging and discharging modes, respectively (Sadeghitabar et al., 2025).

$$SOC_C(t) = P_{bat}(t-1)*(1-\sigma)+\left[\left(P_{Ren}(t)\right)-\frac{D_{Load}(t)}{\eta_{inv}}\right]*\eta_{Gbat} \tag{7}$$

$$SOC_D(t) = P_{bat}(t-1)*(1-\sigma)+\frac{\left[P_{Ren}(t)-\frac{D_{Load}}{\eta_{inv}}\right]}{\eta_{Dbat}} \tag{8}$$

2.4. Converter

In hybrid energy systems, the converter plays a crucial role in coordinating the AC and DC outputs of various components. The inverter's capacity can be defined as shown below (Singh et al., 2016) where η_{inv} represents the inverter efficiency (%), and f_{fim}corresponds to the maximum load demand (kW), which directly affects the sizing of the converter.

$$P_{inv}(t) = \frac{P_m^L(t)}{\eta_{inv}} \tag{9}$$

The power output of a WT is determined using hourly wind speed data in conjunction with the turbine's power curve. Eqs. (10) through (12) define the actual power output (P_{WT}) in kilowatts, based on the specifications provided by the turbine manufacturer (Toopshekan et al., 2022), Eq. (13) presents the theoretical power output of the wind turbine. In this expression, Vdenotes the actual wind speed (m/s), $Y_{WT}$is the turbine's rated capacity (kW), Arefers to the swept area of the blades (m^2), ρrepresents the air density at the designated hub height (kg/m^3), and C is the power coefficient of the turbine. Subsequently, Eq. (14) is used to estimate the total potential renewable energy generation.

$$P_{WT} = \begin{cases} P_{WT} = 0 & V < V_{cut-in} \\ P_{WT} = a.V^3 - b.Y_{WT} & V_{cut-in} < V < V_{rated} \\ P_{wT} = P_{WT} & V_{rated} < V < V_{cut-off} \\ P_{wT} = 0 & V > V_{cut-off} \end{cases} \tag{10}$$

$$a = \frac{Y_{WT}}{V_{rated}^3 - V_{cut-in}^3} \tag{11}$$

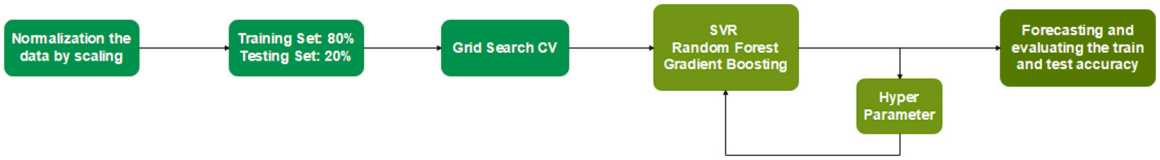

Fig. 4. flowchart of machine learning models.

$$b = \frac{V_{cut-in}^3}{V_{rated}^3 - V_{cut-in}^3} \tag{12}$$

$$P_{WT.theory} = \frac{1}{2}\rho.C.A.V^3 \tag{13}$$

$$P_{Renewable} = P_{PV}\eta_{inv} + P_{WT} \tag{14}$$

In HOMER, data are refreshed at each time interval set to one hour in this case. For wind turbines, the wind speed is computed hourly at the hub height, based on the characteristics of the specified wind resource, as outlined below (Javidmehr et al., 2021).

$$U_{hub} = U_{anem}\frac{Ln\frac{Z_{hub}}{Z_0}}{Ln\frac{Z_{Snem}}{Z_0}} \tag{15}$$

In this equation, U_{anem} (m/s) refers to the wind speed measured at the anemometer height, Z_{hub} (m) is the elevation of the wind turbine hub, Z_0 (m) represents the surface roughness length, and Z_{anem} (m) is the height of the anemometer. It is important to note that the WT does not generate power when wind speeds fall below the cut-in threshold or exceed the cut-out limit. Based on the wind speed at hub height and the turbine's power curve, the WT output is initially calculated under standard conditions. To reflect actual operating conditions, a density correction factor is applied to determine the real power output (Baneshi et al., 2016).

$$P_{WTG} = \left(\frac{\rho}{\rho_0}\right)P_{WTG,STP} \tag{16}$$

Under standard temperature and pressure conditions, the wind turbine's generated power and air density are denoted as $P_{WTG,STP}$ (kW) and ρ_0 (kg/m^3), respectively. The actual air density is represented by ρ(kg/m^3), and the ratio ρ/ρ_0can be calculated using the ideal gas law.

$$\rho = \frac{P}{RT} \tag{17}$$

$$\frac{\rho}{\rho_0} = \frac{P}{P_0}\frac{T_0}{T} \tag{18}$$

Assuming a linear decrease in temperature with altitude up to 11,000 m, as described by the US Standard Atmosphere model, the air density can be expressed accordingly (Akhtari and Baneshi, 2019).

$$T = T_0 - B_Z \tag{19}$$

$$\frac{\rho}{\rho_0} = (1 - \frac{B_Z}{T_0})^{\frac{g}{RB}}\left(\frac{T_0}{T_0 - B_Z}\right) \tag{20}$$

Within these equations, T(K) denotes the actual temperature, while T_0(K) refers to the temperature under standard conditions. R(J/kg·K) is the specific gas constant, P(Pa) represents the atmospheric pressure, and P_0(Pa) is the reference pressure at standard conditions. The lapse rate is indicated by B(K/m), z(m) corresponds to the altitude, and g(m/s^2) is the acceleration due to gravity.

LCOE and NPC are the two primary indicators used in economic evaluations, as they represent the core financial goals in energy system development. Their computation is outlined in Eq. (21) (Oueslati, 2023; Oueslati and Fezai, 2024; Oueslati and Toumi, 2024). The LCOE calculated by dividing the annualized cost of producing electricity Cann,tot ($/yr) by the total power servedEserved (kWh/yr) (Saberi et al., 2024).

$$\text{LCOE} = \frac{C_{ann.total}}{E_{Load,Served}} \tag{21}$$

The LCOE is determined by dividing the total annualized electricity production cost, $C_{ann,tot}$ ($/year), by the total energy delivered, E_{served} (kWh/year).

While these parameters provide an overview of the system's economic performance, the cost-effectiveness of each individual component can be evaluated by calculating its LCOE, using the component-specific cost $C_{Component}$ and its corresponding energy output $E_{Component}$, as defined in Equation 30 (Mousavi et al., 2021).

$$LCOE = \frac{C_{component}}{E_{component}} \tag{22}$$

The SCOE is calculated using Eq. 23, where $C_{ann.total}$ is the total annual cost of the system, and E_{Useful} is the annual useful energy consumed by users (kWh).

$$SCOE = \frac{C_{ann.total}}{E_{useful}} \tag{23}$$

The RF is defined as the share of effective renewable energy specifically, the total renewable power utilized either to meet the load directly or stored in batteries for future use relative to the overall energy produced, as formulated in Eq. 24 (Sadeghitabar et al., 2025).

$$\text{RF} = \frac{E_{Renewable.useful}}{E_{total}} \tag{24}$$

2.5. Machine learning models

As shown in Fig. 4 The dataset underwent normalization to improve processing efficiency and aid the models in recognizing patterns effectively. Following this, the data was split into two categories, training and testing, with an 80:20 ratio to be able to evaluate the trained model by the 20 % of the data. To optimize hyperparameters, Grid Search CV was employed to assess

the performance of various parameters on the model, ultimately identifying the most effective option among those evaluated. The accuracy of the model's performance was measured using the R-Squared metric, which involved analyzing the discrepancies in accuracy between the training and testing results for each model.

The datasets were gathered from the Kaggle website and analyzed to be aware of the influence of each feature on power production, and to have a better accuracy the less important features were removed based on the correlation matrixes shown in Fig. 5. Although the dataset was obtained from Kaggle and the exact site location is not disclosed due to confidentiality agreements, it represents real operational data. To ensure transferability to the Lusail case study, after training and testing the model on this dataset, the meteorological inputs were replaced with real Lusail data. Since the machine learning algorithms primarily learn the relationships between features, updating the input data with site-specific values allowed the model to generate results that are representative of the Lusail context. It should be noted that the Lusail WWTP does not currently have on-site renewable energy installations such as PV or wind turbines; therefore, the renewable generation component in this study is scenario-based, intended to explore the potential

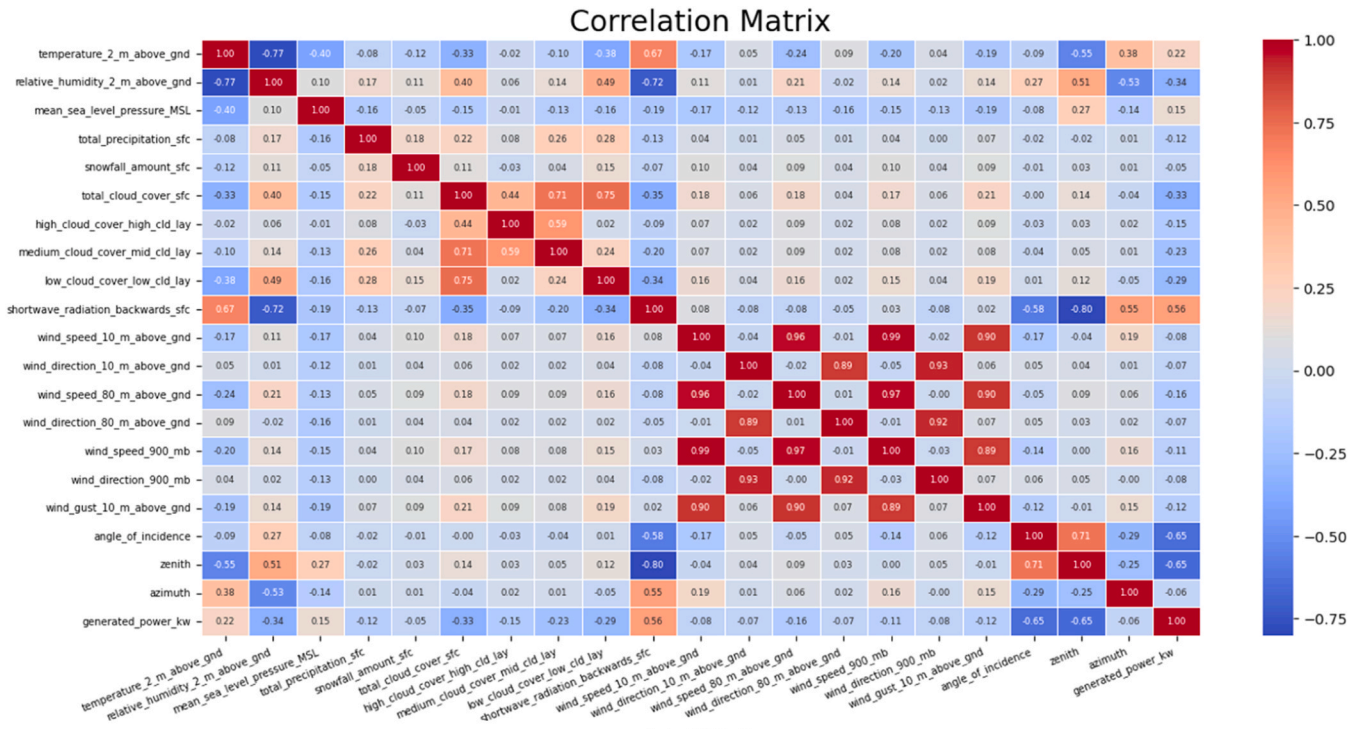

(a) PV dataset

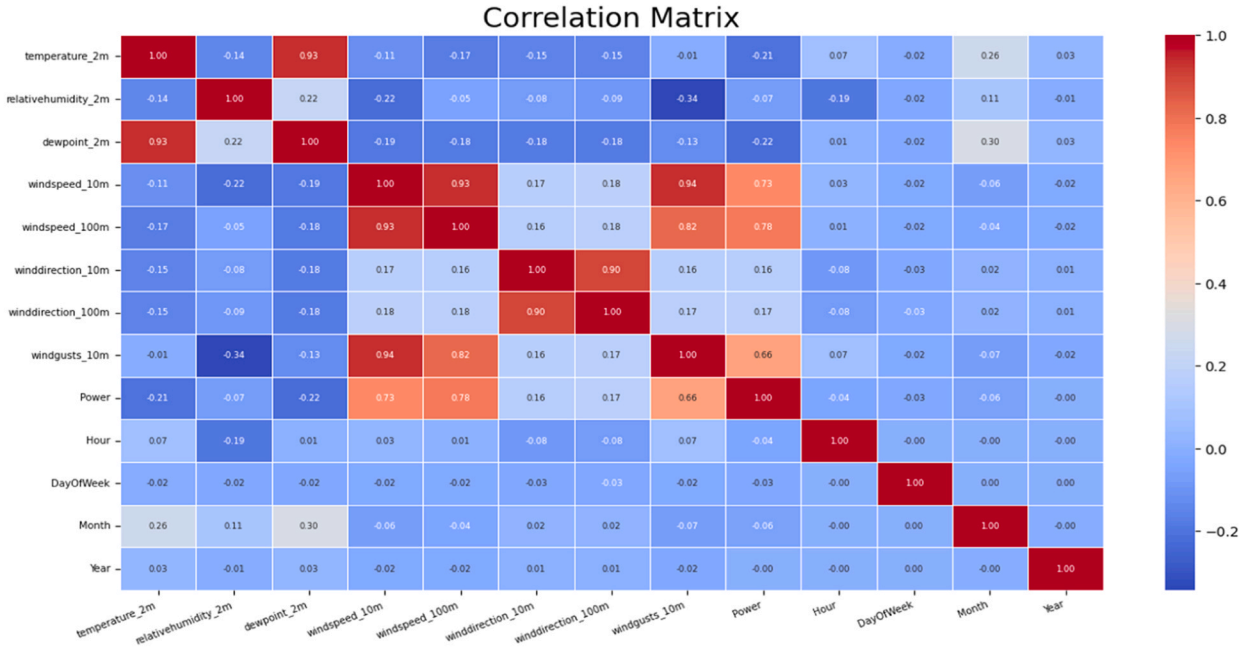

(b)Wind turbine dataset

Fig. 5. The heat map of correlation matrix: (a) PV dataset (b)Wind turbine dataset.

integration of such systems in the future. The PV dataset consists of 21 variables with 4214 observations, although the exact timespan of these measurements is not specified. The wind turbine dataset comprises 10 variables and 43,801 observations, with records beginning on January 2, 2017, though the end date is not indicated. To enhance model interpretability and reduce dimensionality, feature selection was applied to both datasets: the number of PV features was reduced as summarized in Table 3, while the wind dataset was streamlined from 10 to 7 features. This preprocessing ensured that the models focused on the most informative variables, thereby improving computational efficiency and predictive robustness. The correlation analysis revealed that the features closer to −1 indicate a negative correlation, meaning they have

Table 3
Selected features based on correlation matrix.

	PV	Wind turbine
Selected Features	Temperature Relative Humidity Pressure Snowfall Wave Radiation Wind Speed Angle of Incidence Zenith Azimuth	Temperature Relative Humidity Dew Point Wind Speed at 10 m Wind Speed at 100 meter Wind Gust

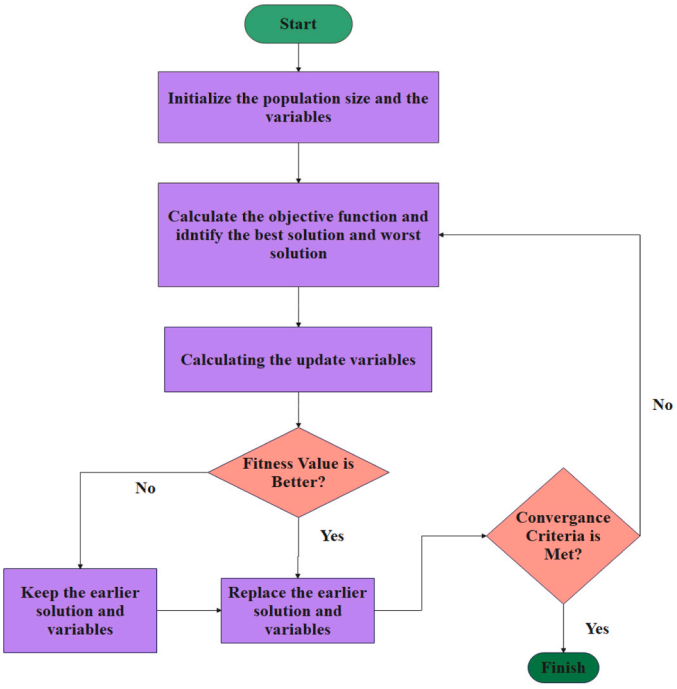

Fig. 6. Jaya flowchart.

an inverse effect on the target function, while those closer to 1 indicate a positive correlation. Additionally, three distinct models were employed, Random Forest, Gradient Boosting Decision Tree, and Support Vector Regression. To be more, Grid Search CV was utilized to determine the most suitable hyperparameters for each model.

2.6. The Jaya algorithm

The Jaya algorithm was used for economic analysis as illustrated in Fig. 6. The algorithm functions by iteratively improving a population of candidate solutions based on the principle of survival of the fittest (Xu et al., 2023). It encourages movement toward the best-known solution while steering clear of the worst solutions, thus balancing exploration and exploitation in the search process (Kader and Zamli, 2020).

We seek to minimize the combined LCOE for a hybrid PV + wind system, accounting for both served load and surplus sales. This minimization is cast as the objective function of the Jaya algorithm. Jaya explores four continuous decision variables: capital cost ($/kW) - operation and maintenance cost ($/kW·yr) each variable is bounded by a realistic range forming the search space for Jaya.

Fixed Inputs such as annual generation (kWh/year) - Installed capacities (kW) Demand and pricing Daily load (kWh/day) - Surplus sale price ($/kWh) and economic parameters for instance: Discount rate - Asset lifetimes.

Annualized Cost Components: CRF To convert upfront capital into an equivalent annual payment, which is showed in Eq. (1′):

$$\mathrm{CRF} = \frac{i(1+i)^n}{(1+i)^n - 1} \tag{1′}$$

i is the discount rate, n is asset lifetime.

Annualized costs are calculated by Eqs. (2′),(3′) and (4′):

$$C_{cap} = capital\ cost \times Capacity_{kW} \times \mathrm{CRF} \tag{2′}$$

$$C_{om} = operation\ and\ maintainece \times Capacity_{kW} \tag{3′}$$

$$C_{total} = C_{cap} + C_{om} \tag{4′}$$

The objective function is calculated by Eq. (5):

$$\mathrm{LCOE} = \frac{Total\ Cost - (Surplus\ electricity \times Sell\ Price)}{Generated\ Electricity} \tag{5′}$$

Moreover, the Table 4 is provided to ilusstrate the strength, limitation and use case of the selected algorithms.

3. Results

3.1. Simulation results

The Four scenarios of simulation is discussed:

3.1.1. Scenario 1 (Renewable source without batteries)

Fig. 7 demonstrates a seasonal variation in electricity production, with peak generation occurring at the end of spring and during the summer months, primarily due to increased PV output under higher solar irradiance. The G1500 (WT) system consistently contributes a significant portion of the monthly electricity supply, confirming its reliability as a baseline energy source throughout the year. The grid's supplementary role, particularly evident during months of reduced PV generation, indicates an effective balance between renewable and non-renewable energy sources.

From an operational perspective, these seasonal patterns can guide WWTP managers in scheduling energy-intensive processes, such as aeration or sludge treatment, during periods of higher renewable output to minimize grid dependence and operational costs. Additionally, recognizing the seasonal decline in PV production highlights the need for strategic battery management and predictive maintenance planning

Table 4
advantages, disadvantages, and use cases of selected algorithms.

Algorithm	Strengths	Limitations	Use Cases	References
SVR	Handling Nonlinearity - Versatility	Parameter Selection - Computational Cost	Industrial Applications - Financial Forecasting	(Xu, 2024; Ji and Bende, 2007; Farahmand et al., 2014; Das et al., 2025)
Random Fores	Robustness - Versatility	Computational Cost - Model Interpretability	Feature Selection - Environmental Studies	(Pious et al., 2024; Rodriguez-Galiano et al., 2014; Wang, 2023)
Gradient Boosting	Flexibility	Overfitting - Training Time	Feature Importance -Environmental Studies	(Liu et al., 2024; Kulhare, 2024; Reddy and Kumar, 2023; Tomas et al., 2022)
Jaya	Parameter-Free - Global Optimization	Local Optima - Premature Stagnation	Engineering Design - Power Systems	(Barakat et al., 2018; Peng et al., 2025; Grzywiński et al., 2023)

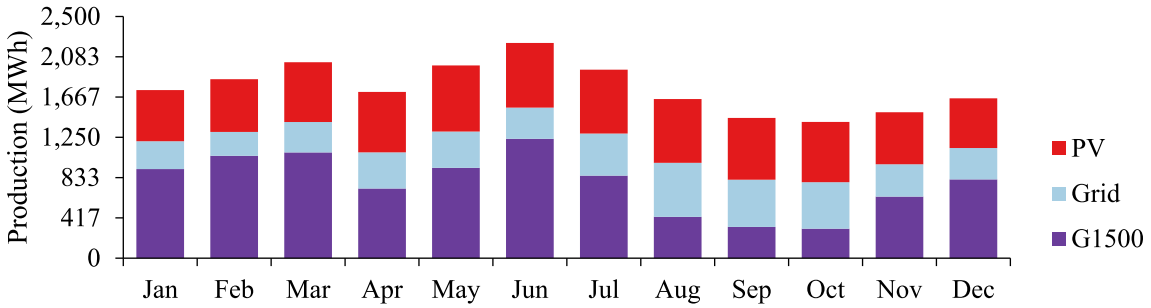

Fig. 7. Monthly Electricity Production Breakdown by Source: PV, Grid, and G1500 (WT) Systems.

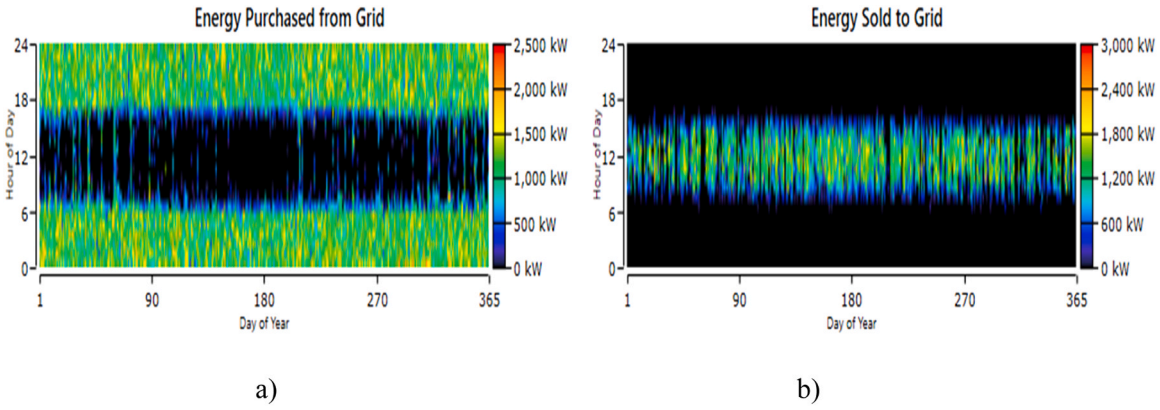

Fig. 8. Analysis of the pattern of a) buying and b) selling energy from the network throughout the year.

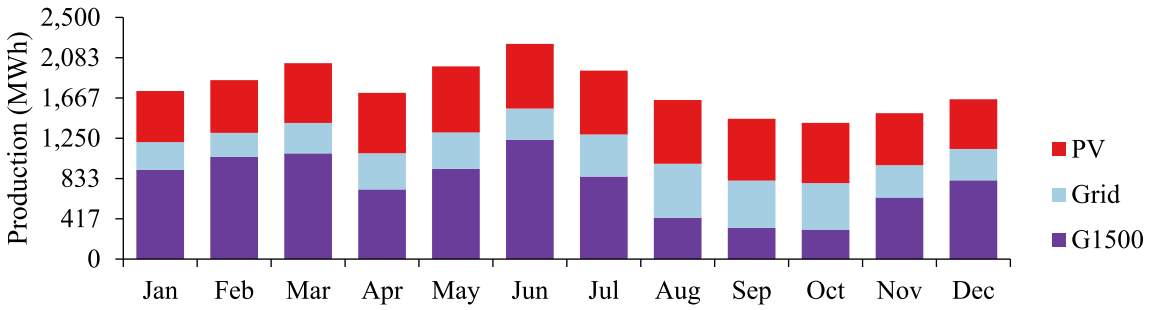

Fig. 9. Monthly Electric Production.

to ensure uninterrupted operation during low-solar months. Overall, the results emphasize that hybrid energy systems not only support sustainability goals but also provide actionable insights for optimizing WWTP energy management and cost-efficiency across different seasons.

Fig. 8, part a depicts the energy purchased from the grid over time, providing a clear indication of reliance on external power sources. The data shows fluctuations in energy procurement, which can be attributed to varying demands placed on the WWTP throughout different periods. Part b indicates specific times when energy demand exceeds local generation capacity, necessitating increased purchases from the grid. This is particularly relevant during periods of low renewable output, such as cloudy days or nighttime. Frequent reliance on grid energy can lead to higher operational costs, emphasizing the importance of integrating renewable sources to mitigate expenses and enhance sustainability. The ability to purchase energy from the grid allows for operational flexibility, ensuring that treatment processes remain uninterrupted even during periods of low renewable generation. The results suggest that implementing predictive control strategies and energy storage management could enhance grid interaction efficiency and stabilize operation under variable renewable conditions. The overall COE for this configuration was 0.137 $/kWh.

3.1.2. *Scenarios 2(a) and 2(b) (Renewable sources with batteries)*

This Fig. 9 illustrates the monthly electricity production, categorized by sources: PV (solar photovoltaic), Grid, and G1500 (Wind turbine). The production levels vary throughout the year, with higher total energy production observed in spring and early summer months, particularly in June. Solar PV contributes consistently, especially during sunnier months, while reliance on grid energy is prominent across all months. This data can provide insights for optimizing energy management by balancing renewable sources and grid dependency to achieve cost and sustainability goals.

In this section, although the system includes a battery, it was not utilized for charging due to the low cost of purchasing electricity from the grid, priced at 0.036 $/kWh. Instead, it was more cost-effective to forego battery charging entirely and sell the surplus generated power back to the grid at a rate of 0.035 $/kWh.

According to the sensitivity analysis, utilizing a battery is not cost-effective unless the grid electricity purchase price reaches 0.45 $/kWh, known as Scenario 2(b) in this paper.

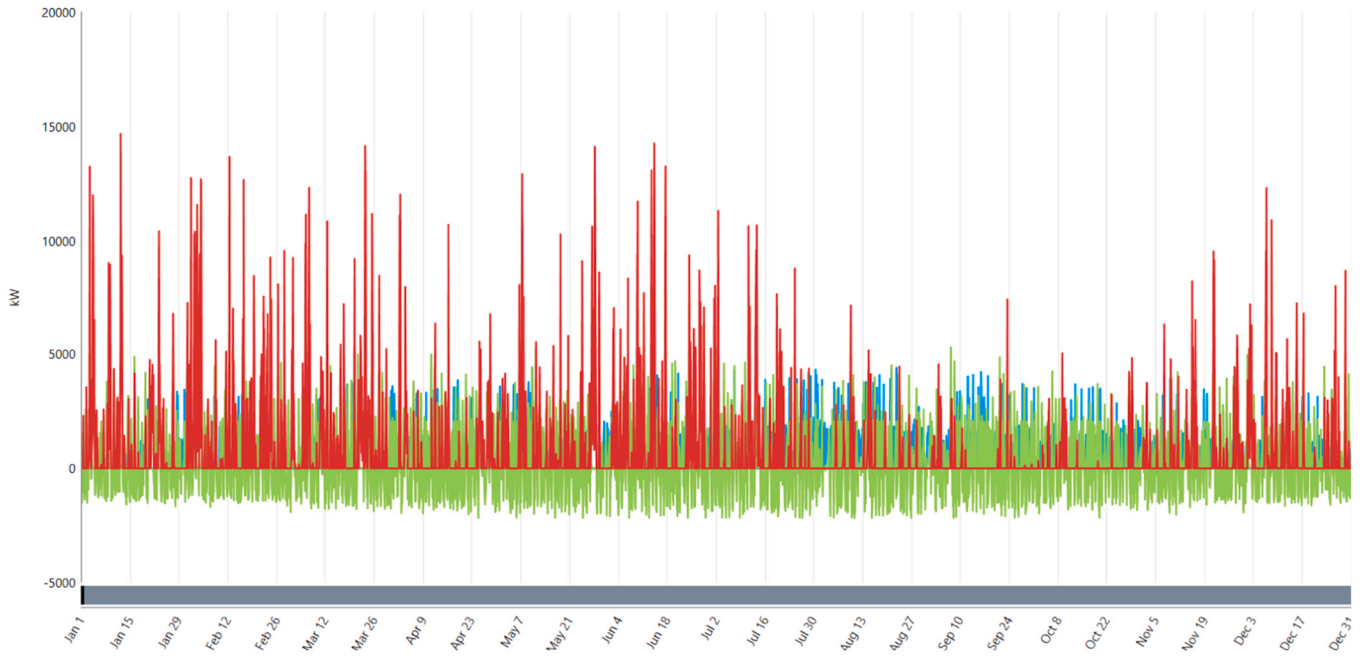

Fig. 10. Battery usage.

Table 5
Results of the simulations.

	NPC (million dollars)	LCOE ($/kWh)	Renewable Fraction
Scenario 1	40.9	0.14	77.8 %
Scenario 2 (a)	41	0.14	77.9 %
Scenario 2 (b)	67.3	0.284	91.2 %

Table 6
Performance and Prediction Values of Machine Learning Based on Energy Source Dataset.

ML Models	Train R2-Square	Test R2-Square	Overfit Rate	Energy Source
SVR	0.75	0.73	0.02	Solar
Random Forest	0.91	0.79	0.12	
Gradient Boost	0.90	0.79	0.11	
SVR	0.68	0.67	0.01	Wind
Random Forest	0.90	0.69	0.21	
Gradient Boost	0.76	0.68	0.08	

In Scenario 2(b), Fig. 10 presents a detailed time series analysis of power sources throughout the year. The x-axis spans from January to December, while the y-axis indicates power values in kW. The figure's legend identifies the different power flows: energy input and output to a 1 kWh lead-acid battery (green), power sold to the grid (red), and power purchased from the grid (blue). Although the battery is integrated into the system, the figure illustrates that surplus power is predominantly exported to the grid rather than stored for later use by the desalination site. This trend suggests a potential mismatch between the generated power and the storage capacity, indicating that the current configuration may not be optimal for effective onsite energy utilization.

To provide a clearer comparison of the scenario outcomes, Table 5 summarizes the key results. As evident from the table, incorporating a battery is not cost-effective in terms of both NPC and LCOE. The use of battery storage significantly enhances the ability of renewable generators to supply power across different hours, contributing to improved sustainability and load balancing. From an operational perspective, this higher renewable contribution reduces dependence on the grid during peak demand or low-generation periods, improving energy reliability for WWTP operations. This finding suggests that, although batteries are currently less viable economically, their long-term value lies in supporting stable, low-carbon operations, particularly if future policy measures, such as improved sellback prices or battery incentives, are introduced.

3.2. *Machine learning prediction results*

According to Table 6, it can be observed that the SVR model exhibits weaker performance with the dataset. It demonstrates robustness against overfitting compared to other models. Despite the potential for some overfitting in the other two models, they achieve better accuracy given the number of samples available in the dataset.

The predicted values from both the Random Forest and Gradient Boosting models show a strong correlation, particularly evident in the solar dataset.

Based on the results of each model Gradient Boosting was selected to be used to predict energy production and the result is showed in Fig. 11, it can be understand that wind source is more reliable compared to solar. The optimization performed using the Jaya algorithm yielded a COE that converged to 8.41 $/kWh, while achieving a renewable energy penetration of 20.39 % with a system of comparable scale to the previous scenarios. This elevated COE can be partly attributed to the fact that the dataset used for training the machine learning model was not of high quality, which is reflected in the model's accuracy metrics. To mitigate this, we applied feature reduction techniques, and CV to improve performance, though some limitations remain. Although, This outcome contrasts sharply with the earlier simulation-based result, primarily because the Jaya method employs a heuristic search strategy rather than a deterministic simulation. As a consequence, the renewable penetration in the Jaya-derived solution is 57.51 % lower than that obtained via first scenario and also, the total electricity output predicted under the machine learning method is approximately one-eighth of that produced in the first scenario.

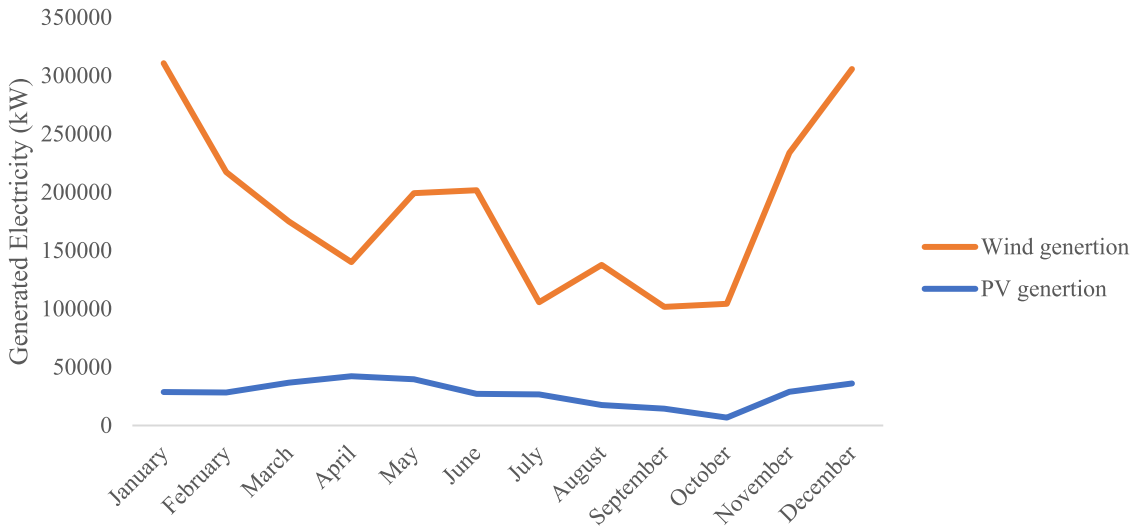

Fig. 11. predicted energy based on equipment.

4. Conclusion

Supplying reliable energy to high-consumption facilities such as wastewater treatment plants is essential for the sustainable growth of modern cities. Integrating clean energy generation into these facilities not only reduces dependence on conventional grid electricity but also delivers measurable economic and environmental benefits. This study advances beyond traditional HOMER-based analyses by combining three deterministic scenarios simulated in HOMER with a stochastic scenario developed through a novel hybrid Machine Learning–Metaheuristic framework. Unlike prior work, this dual approach captures both baseline techno-economic performance and the uncertainties arising from data quality and system variability. By benchmarking results against grid electricity prices and exploring hypothetical sellback conditions, the study highlights the practical applicability of the findings and underscores their significance for future energy planning in Qatar and similar contexts. Key contributions and results are summarized as follows:

- The results revealed a substantial divergence between deterministic and stochastic modeling outcomes. Specifically, the deterministic models produced LCOE of 0.14$/kWh and0.284 $/kWh , values that are broadly consistent with benchmarks reported in previous renewable integration studies under average operating conditions. In contrast, the stochastic hybrid model yielded a markedly higher LCOE of 8.41 $/kWh, reflecting the explicit incorporation of uncertainty in meteorological inputs, renewable intermittency, and operational variability. This discrepancy highlights the critical importance of adopting stochastic approaches when evaluating renewable energy integration in WWTPs, as deterministic models may underestimate costs by smoothing over variability. The finding underscores the novelty of this study in demonstrating, quantitatively, how risk-aware modeling can alter the economic feasibility assessment and provide more conservative, yet operationally realistic, insights for decision-makers.
- The most positively influenced parameter for predicting PV energy production is short wave radiation on the surface, while the zenith angle has the most negative impact. For wind turbines, wind speed at 100 m height has the strongest positive impact, while the dew point exerts the most negative influence.
- Among the four scenarios, wind turbines demonstrate stronger potential to meet energy demands, as the energy produced by wind (from the Machine Learning model) is 5.7 times greater than that of PV systems. It is essential to evaluate the limitations associated with site selection for wind turbines in the region.
- The analysis further revealed that the contribution of battery storage to the system was negligible under current cost conditions. Only when the purchase price of renewable electricity decreases to approximately 0.45 $/kWh does battery deployment become economically viable. This threshold highlights the sensitivity of storage integration to market prices and underscores the importance of future cost reductions, policy incentives, or technological advancements in making batteries a competitive option for wastewater treatment plants.
- The hybrid Machine Learning–Metaheuristic optimization model demonstrated that, under current market conditions in Qatar, supplying energy from a hybrid renewable configuration is not economically feasible. The analysis assumed a grid electricity purchase price of 0.036 $/kWh and a hypothetical sellback price of 0.035 $/kWh, since no official feed-in tariff currently exists. This assumption was introduced solely for modeling purposes to explore potential economic outcomes. The results indicate that, given the present tariff structure, hybrid renewable systems cannot compete with grid electricity. Their viability would therefore depend on either substantial reductions in renewable technology costs or the introduction of supportive policy mechanisms, such as feed-in tariffs, subsidies, or carbon pricing, to improve competitiveness.

4.1. Suggestions

The sellback rate used in this study is a hypothetical value for scenario analysis, as Qatar currently lacks a formal feed-in tariff policy. This assumption enables exploration of future pricing structures and their impact on system viability. The finding that battery systems become economically viable only when the sellback price reaches approximately 0.45 $/kWh highlights the critical role of governance and policy design in promoting renewable integration. In future scenarios, the implementation of dynamic pricing schemes, renewable energy incentives, or feed-in tariffs could help achieve such sellback rates, thereby enhancing the economic attractiveness of battery storage in renewable-based systems. One of the key challenges encountered in this research was the difficulty of accessing high-quality datasets specific to the WWTP context. To address this, we applied feature reduction techniques to minimize the influence of less relevant variables, but further improvements could be achieved through enhanced data collection strategies, such as integrating smart metering, sensor-based monitoring, and long-

term site-specific measurements. Future research should also consider data preprocessing methods, such as outlier detection, normalization, and data augmentation, to improve dataset robustness and ensure more reliable model outcomes.

CRediT authorship contribution statement

Alireza Ahmadi: Writing – original draft, Methodology, Formal analysis, Conceptualization. **Mahmood Abdoos:** Resources, Formal analysis, Data curation. **Ali Roghani Araghi:** Writing – review & editing, Validation, Project administration. **Amir Ali Saifoddin:** Supervision, Investigation.

Consent to Participate

We affirm that all authors have participated in the research work and are fully aware of ethical responsibilities.

Consent to Publish

We affirm that all authors have agreed to submit the paper to Energy Reports and are fully aware of ethical responsibilities.

Ethical Approval

We confirm that the manuscript entitled "**Energy Forecasting and Optimization for Wastewater Treatment Facility: A Hybrid Machine Learning – Metaheuristic Scenario Based Approach**", it has been absolutely our main work. It implies Energy Reports that were not previously published.

Funding

Funding information is not applicable / No funding was received.

Declaration of Competing Interest

The authors declare that they have no known competing financial interests or personal relationships that could have appeared to influence the work reported in this paper.

Data Availability

Data will be made available on request.

References

Ahmadi, A., et al., 2025. Techno-economic comparison of battery–flywheel with battery–hydrogen storage system in the vicinity of off-grid HRES for four climates: MCDM method. Energy Sci. Eng. 13 (5), 2512–2529.

Akhtari, M.R., M.J.E.C. Baneshi, and Management, Techno-economic assessment and optimization of a hybrid renewable co-supply of electricity, heat and hydrogen system to enhance performance by recovering excess electricity for a large energy consumer. 2019. 188: p. 131-141.

Alvarez-Guerra, E., Dominguez-Ramos, A., Irabien, A., 2011. Photovoltaic solar electro-oxidation (PSEO) process for wastewater treatment. Chem. Eng. J. 170 (1), 7–13.

Ashtiani, M.N., et al., Techno-economic analysis of a grid-connected PV/battery system using the teaching-learning-based optimization algorithm. 2020. 203: p. 69-82.

Baneshi, M., F.J.E.C. Hadianfard, and Management, Techno-economic feasibility of hybrid diesel/PV/wind/battery electricity generation systems for non-residential large electricity consumers under southern Iran climate conditions. 2016. 127: p. 233-244.

Baniasad Askari, I., Ameri, M.J.E.S., 2011. The effect of fuel price on the economic analysis of hybrid (Photovoltaic/Diesel/Battery) systems in Iran. Part B Econ. Plan. Policy 6 (4), 357–377.

Barakat, A.F., et al., 2018. Solving reactive power dispatch problem by using JAYA optimization algorithm. Int. J. Eng. Res. Afr. 36, 12–24.

Bogdanov, D., Toktarova, A., Breyer, C., 2019. Transition towards 100% renewable power and heat supply for energy intensive economies and severe continental climate conditions: Case for Kazakhstan. Appl. Energy 253, 113606.

Dange, S., Arumugam, K., Vijayaraghavalu, S.S., 2025. Unlocking Vellore's water future: Integrated hydrogeochemical research aligns with SDGs 6, 12, and 13. Results Eng. 25, 103852.

Das, J.D., et al., 2025. Hybrid LSTM/GRU and support vector regression models for stock index prediction. 2025 IEEE 49th Annual Computers, Software, and Applications Conference (COMPSAC). IEEE.

Du, X., Peng, Y., 2023. Multi-objective pity beetle algorithm based optimal control of wastewater treatment process. Process Saf. Environ. Prot. 170, 188–206.

Elnakar, H., Buchanan, I., 2019. The role of mixing in potassium ferrate (VI) consumption kinetics and disinfection of bypass wastewater. J. Environ. Manag. 231, 515–523.

Farahmand, M., Desa, M.I., Nilashi, M., 2014. A combined data envelopment analysis and support vector regression for efficiency evaluation of large decision making units. Int. J. Eng. Technol. (IJET) 2310–2321.

Fazelpour, F., N. Soltani, and M.A.J.Ijohe Rosen, Economic analysis of standalone hybrid energy systems for application in Tehran, Iran. 2016. 41(19): p. 7732-7743.

Ghorbani, N., et al., Optimizing a hybrid wind-PV-battery system using GA-PSO and MOPSO for reducing cost and increasing reliability. 2018. 154: p. 581-591.

Grzywiński, M., et al., 2023. Jaya algorithm for optimization of 2D reinforced concrete frame structure. International Conference on Computer Methods in Mechanics and 5th Polish Congress of Mechanics. Springer.

Guangqian, D., et al., A hybrid algorithm based optimization on modeling of grid independent biodiesel-based hybrid solar/wind systems. 2018. 122: p. 551-560.

Hao, X., Liu, R., Huang, X., 2015. Evaluation of the potential for operating carbon neutral WWTPs in China. Water Res. 87, 424–431.

He, L., et al., 2018. Techno-economic potential of a renewable energy-based microgrid system for a sustainable large-scale residential community in Beijing, China. Renew. Sustain. Energy Rev. 93, 631–641.

Heydari, A. and A.J.A.E. Askarzadeh, Optimization of a biomass-based photovoltaic power plant for an off-grid application subject to loss of power supply probability concept. 2016. 165: p. 601-611.

Jahangir, M.H., et al., A techno-economic comparison of a photovoltaic/thermal organic Rankine cycle with several renewable hybrid systems for a residential area in Rayen, Iran. 2019. 195: p. 244-261.

Jahangir, M.H., A. Shahsavari, and M.A.Vaziri Rad, Feasibility study of a zero emission PV/Wind turbine/Wave energy converter hybrid system for stand-alone power supply: A case study. 2020. 262: p. 121250.

Jamshidi, M., A.J.S.C. Askarzadeh, and Society, Techno-economic analysis and size optimization of an off-grid hybrid photovoltaic, fuel cell and diesel generator system. 2019. 44: p. 310-320.

Javidmehr, M., et al., Optimal design and analysis of a district energy system including heat and power production for domestic applications and fuel for vehicles. 2021. 144 (5): p. 2009-2025.

Ji, L., Bende, W., 2007. Parameters selection for SVR based on the SCEM-UA algorithm and its application on monthly runoff prediction. 2007 International Conference on Computational Intelligence and Security (CIS 2007). IEEE.

Kader, M.A., Zamli, K.Z., 2020. Adopting Jaya algorithm for team formation problem. Proceedings of the 2020 9th International Conference on Software and Computer Applications.

Kasaeian, A., et al., Optimal design and technical analysis of a grid-connected hybrid photovoltaic/diesel/biogas under different economic conditions: a case study. 2019. 198: p. 111810.

Kulhare, R., 2024. Gradient Boosting Feature Selection with Machine Learning Classifier for Prediction of Intrusion Image. 2024 4th International Conference on Technological Advancements in Computational Sciences (ICTACS). IEEE.

Liu, Y., et al., 2024. Research on accurate prediction method of epilepsy stage based on gradient boosting algorithm. 2024 12th International Conference on Information Systems and Computing Technology (ISCTech). IEEE.

Maleki, A., et al., A novel framework for optimal photovoltaic size and location in remote areas using a hybrid method: a case study of eastern Iran. 2017. 153: p. 129-143.

Masłoń, A., et al., 2020. The enhancement of energy efficiency in a wastewater treatment plant through sustainable biogas use: Case study from Poland. Energies 13 (22), 6056.

Mehrpooya, M., et al., Techno-economic-environmental study of hybrid power supply system: A case study in Iran. 2018. 25: p. 1-10.

Mohammadi, M., et al., Optimal planning of renewable energy resource for a residential house considering economic and reliability criteria. 2018. 96: p. 261-273.

Mousavi, S.A., et al., Decision-making between renewable energy configurations and grid extension to simultaneously supply electrical power and fresh water in remote villages for five different climate zones. 2021. 279: p. 123617.

Nowak, O., Enderle, P., Varbanov, P., 2015. Ways to optimize the energy balance of municipal wastewater systems: lessons learned from Austrian applications. J. Clean. Prod. 88, 125–131.

Oueslati, F. and S.J.W.E. Fezai, Optimal techno-economic design of PV-wind hydrogen refueling stations (HRFS) for 20 selected Saudi sites. 2024. 48(6): p. 1055-1075.

Oueslati, F., N.J.E. Toumi, Development, and Sustainability, Technical feasibility and financial assessment of autonomous hydrogen refuelling stations fully supplied by mixed renewable energy systems for twenty selected sites located in France. 2024: p. 1-39.

Oueslati, F., HOMER optimization of standalone PV/Wind/Battery powered hydrogen refueling stations located at twenty selected French cities. 2023. 12(6): p. 1070-1090.

Peng, Y., et al., 2025. A fractional-order JAYA algorithm with memory effect for solving global optimization problem. Expert Syst. Appl. 270, 126539.

Pious, I.K., et al., 2024. Enhancing prediction accuracy through random forest in classification and regression. 2024 International Conference on Smart Technologies for Sustainable Development Goals (ICSTSDG). IEEE.
Pochwała, S., Kotas, P., 2018. Possibility of obtaining wastewater heat from a sewage treatment plant by the means of a heat pump–a case study. E3S Web of Conferences. EDP Sciences.
Qiblawey, Y., et al., 2022. Techno-economic assessment of increasing the renewable energy supply in the Canary Islands: the case of Tenerife and Gran Canaria. Energy Policy 162, 112791.
Rad, M.A.V., et al., Techno-economic assessment of a hybrid system for energy supply in the affected areas by natural disasters: A case study. 2020a. 221: p. 113170.
Rad, M.A.V., et al., A comprehensive study of techno-economic and environmental features of different solar tracking systems for residential photovoltaic installations. 2020b. 129: p. 109923.
Rad, M.A.V., et al., Technical and economic evaluation of excess electricity level management beyond the optimum storage capacity for off-grid renewable systems. 2024. 87: p. 111385.
Razmjoo, A., Davarpanah, A.J.E.S., 2019. Developing various hybrid energy systems for residential application as an appropriate and reliable way to achieve energy sustainability. Part A Recovery Util. E. Eff. 41 (10), 1180–1193.
Reddy, P.V., Kumar, S.M., 2023. A novel approach to improve accuracy in stock price prediction using gradient boosting machines algorithm compared with Random Forest algorithm. AIP Conference Proceedings. AIP Publishing LLC.
Rodriguez-Galiano, V., et al., 2014. Predictive modeling of groundwater nitrate pollution using Random Forest and multisource variables related to intrinsic and specific vulnerability: a case study in an agricultural setting (Southern Spain). Sci. Total Environ. 476, 189–206.
Saberi, N., et al., Comparative techno-economic analysis of battery bank and integrated flywheel and generator in a hybrid renewable system under tropical climate. 2024. 103: p. 114145.
Sadeghitabar, E., et al., Optimization and Shannon entropy multi-criteria decision-making method for implementing modern renewable energies in stand-alone greenhouses. 2025. 27: p. 101139.
Shiroudi, A., et al., Stand-alone PV-hydrogen energy system in Taleghan-Iran using HOMER software: optimization and techno-economic analysis. 2013. 15(5): p. 1389-1402.
Singh, S., et al., Feasibility study of an islanded microgrid in rural area consisting of PV, wind, biomass and battery energy storage system. 2016. 128: p. 178-190.
Talaie, A., Kamyab, H., Razmfarsa, A., 2024. Advancing environmental engineering: the role of artificial intelligence in sustainable solutions-a short review. J. Environ. Treat. Tech. 12 (3).
Tomas, J.P.Q., et al., 2022. Classification of flood disaster risks with the use of gradient boosting algorithm. Proc. 2022 5th Int. Conf. Comput. Intell. Intell. Syst.
Toopshekan, A., et al., Evaluation of a stand-alone CHP-Hybrid system using a multi-criteria decision making due to the sustainable development goals. 2022. 87: p. 104170.
Viet, N.D., et al., 2019. Enhancing the removal efficiency of osmotic membrane bioreactors: A comprehensive review of influencing parameters and hybrid configurations. Chemosphere 236, 124363.
Wang, H., 2023. Research on the application of Random Forest-based feature selection algorithm in data mining experiments. Int. J. Adv. Comput. Sci. Appl. 14 (10).
Xiong, Y.-T., et al., 2021. Geographic distribution of net-zero energy wastewater treatment in China. Renew. Sustain. Energy Rev. 150, 111462.
Xu, J., et al., 2023. A discrete JAYA algorithm based on reinforcement learning and simulated annealing for the traveling salesman problem. Mathematics 11 (14), 3221.
Xu, K., 2024. Industrial steam quantity prediction model based on grid search-optimized support vector regression. 2024 IEEE 3rd International Conference on Electrical Engineering, Big Data and Algorithms (EEBDA). IEEE.
Zhang, W., et al., Optimization with a simulated annealing algorithm of a hybrid system for renewable energy including battery and hydrogen storage. 2018. 163: p. 191-207.
Zhang, Y., et al., 2024. Machine learning modeling for the prediction of phosphorus and nitrogen removal efficiency and screening of crucial microorganisms in wastewater treatment plants. Sci. Total Environ. 907, 167730.